Accelerated Antibody Discovery Targeting the SARS-CoV-2 Spike Protein for COVID-19 Therapeutic Potential

Authors: Tracey Mullen, Rashed Abdullah, Jacqueline Boucher, Anna Susi Brousseau, Narayan Kumar Dasuri, Andrew Doucette, Chloe Emery, Justin Gabriel, Brendan Greamo, Ketan Patil, Kelly Rothenberger, Justin Stolte, and Colby Souders

Abstract

Rapid deployment of technologies capable of high-throughput and high-resolution screening is imperative for timely response to viral outbreaks. Risk mitigation in the form of leveraging multiple advanced technologies further increases the likelihood of identifying efficacious treatments in an aggressive timeline. In this study, we describe two parallel, yet distinct, *in vivo* approaches for accelerated discovery of antibodies targeting the SARS-CoV-2 spike protein. Beginning with human transgenic Alloy-GK mice, we detail a single B-cell discovery workflow to directly interrogate antibodies secreted from plasma cells for binding specificity and ACE2 receptor blocking activity. Additionally, we describe a concurrent accelerated hybridoma-based workflow utilizing a DiversimAb™ mouse model for increased diversity. The panel of antibodies isolated from both workflows revealed binding to distinct epitopes with both blocking and non-blocking profiles. Sequence analysis of the resulting lead candidates uncovered additional diversity with the opportunity for straightforward engineering and affinity maturation. By combining *in vivo* models with advanced integration of screening and selection platforms, lead antibody candidates can be sequenced and fully characterized within one to three months.

Introduction

The global pandemic caused by severe acute respiratory syndrome coronavirus-2 (SARS-CoV-2), or coronavirus disease 2019 (COVID-19), has received unprecedented attention from the scientific community in an effort to rapidly develop efficacious treatments and vaccines. Within weeks of the emergence of viral pneumonia outbreaks in Wuhan, China, deep sequencing had identified the cause,[1] and the resulting mobilization of widespread therapeutic and prophylactic discovery efforts ensued. The response to the COVID-19 pandemic mirrored that of other recent viral outbreaks, including, but not limited to, H1N1 influenza in 2009,[2] Ebola Virus in 2014,[3,4] and Zika Virus in 2015.[5] Lessons learned from these public health threats helped guide the strategy for the accelerated response to COVID-19. In particular, the understanding that neutralizing antibody function is fundamental to combating disease progression[6] helped streamline early antibody-based drug therapy discovery strategies.

Beyond direct therapeutic use, antibodies can help inform vaccine design to enable next-generation vaccine development with a focus on relevant viral epitopes.[7] In general, the most valuable and broadly applicable antiviral antibodies are those that exhibit cross-reactivity to related viruses and are unaffected by escape mutant evolutionary pressures.[8] These antibodies, which can function either alone or in combination with oligoclonal mixtures of non-competing antibodies,[9] harbor basic properties like receptor blocking activity and high affinity. When taken in aggregate, these criteria are quite stringent and therefore necessitate efficient, high-

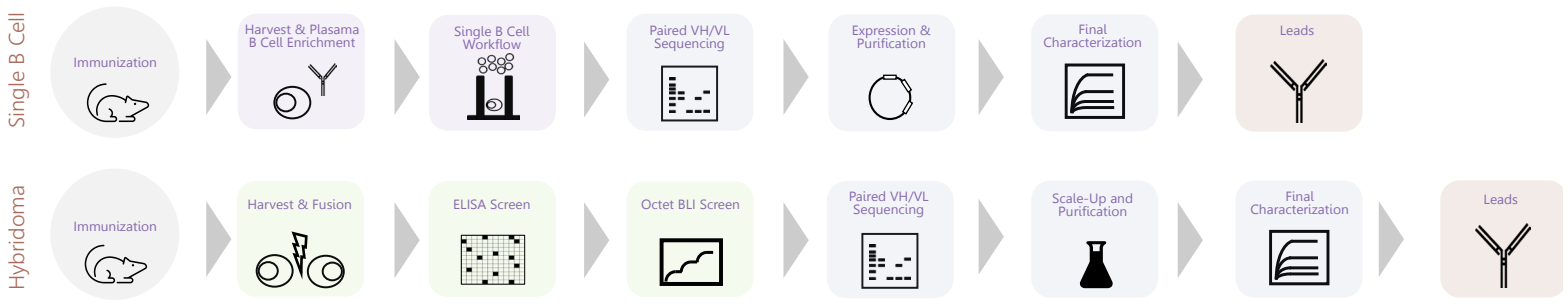

Figure 1. Overview of the process followed for two parallel upstream discovery workflows employed for rapid antibody discovery.

resolution screening strategies to identify valuable lead candidates.

This report highlights several different techniques and antibody discovery workflows leveraged in the discovery and characterization of antibody panels targeting the spike protein (S) of SARS-CoV-2. Across the different workflows, two separate mouse strains were immunized with the S1 subunit (which contains the receptor binding domain): a humanized strain to facilitate the discovery of fully human antibodies (Alloy GK mice), and an engineered mouse strain designed to elicit greater epitopic diversity and overall immune response (Abveris DiversimAb™ mice). Furthermore, two distinct upstream discovery methods were applied (Figure 1): a hybridoma discovery platform optimized for high-content screening and efficiency (Abveris Hybridoma Workflow), and a high-throughput state-of-the-art single B cell screening platform (Abveris Single B Cell Worflow enabled by the Berkeley Lights Beacon®). Final characterization and candidate analysis was performed on the Carterra LSA™.

Methods and Results

Immunization of DiversimAb and Alloy GK mice was completed in 16 and 35 days, respectively; both protocols resulted in an appreciable immune response as indicated by detectable serum titer to the S and S1 proteins at serum dilution factors of at least 1:70,000 or higher (data not shown). Following a high-efficiency electrofusion to generate hybridoma lines, resulting colonies were initially screened by ELISA to identify S protein-reactive clones. Preliminary clones of interest were subsequently screened via high-throughput biolayer interferometry (BLI) kinetic screening on the ForteBio Octet® system to select candidates for scale up and antibody purification from hybridoma cultures. Simultaneously, sequencing of immunoglobulin genes was performed following a high-throughput hybridoma sequencing procedure and

Table 1. Binding characteristics of anti-S protein candidates, including ELISA binding, single point kinetic measurements to the trimeric S protein, affinity characterization to the monomeric S1 protein and effect on ACE2 binding to S1 protein (S1:ACE2 interaction blocking activity).

	Indirect ELISA (OD 450nm)		BLI Kinetics (ForteBio); Trimeric S Protein (100nM)				SPR Kinetics (Carterra); Monomeric S1 Protein (500nM, 125nM, 31.25nM, 7.81nM, 1.95nM, 0.49nM)					S1:ACE2 Interaction (Carterra)
ID	S Protein (+)	Irrelevant AVI-His Tagged Protein (-)	ka (M^{-1} s^{-1})	kd (s^{-1})*	KD (nM)**	R^2	ka (M^{-1} s^{-1})	kd (s^{-1})	KD (nM)	R_{max}	Res sd	% Change ACE2 Binding***
15G11	0.879	0.041	1.05E+05	2.23E-03	21.3	0.9582	3.23E+04	1.12E-03	38.50	154	7.725	51.95
16F2	1	0.04	8.85E+04	<1E-05	<1	0.9924	7.13E+04	8.50E-04	12.58	326	8	-7.73
18F4	1.05	0.042	7.03E+04	<1E-05	<1	0.9467	6.95E+04	4.65E-04	7.48	299	7.025	-3.44
1E5	1.216	0.041	1.10E+05	<1E-05	<1	0.9522	1.30E+05	5.78E-04	5.73	246	11.725	16.55
1G3	0.818	0.041	6.32E+04	<1E-05	<1	0.958	3.85E+04	6.55E-04	18.00	250	10.45	3.77
21C3	0.81	0.043	7.18E+04	<1E-05	<1	0.9872	3.68E+04	6.63E-04	19.50	269	8.425	-1.27
22D9	0.8	0.042	7.63E+04	<1E-05	<1	0.9866	6.30E+04	6.08E-04	11.83	295	11.6	-0.43
23D11	1.241	0.042	9.03E+04	1.13E-04	1.25	0.9903	1.20E+05	1.09E-03	9.73	234	8.325	3.34
26E2	1.113	0.044	8.23E+04	1.66E-03	20.2	0.9871	8.08E+04	1.11E-03	14.25	290	13.25	44.66
29F7	0.714	0.041	1.12E+05	1.63E-04	1.46	0.9267	5.13E+04	3.55E-04	7.88	335	9.725	52.71
3B3	1.100	0.041	8.39E+04	1.19E-03	14.2	0.9852	6.10E+04	5.40E-04	10.10	250	11.75	35.91
3F2	1.261	0.045	9.26E+04	<1E-05	<1	0.9539	1.60E+05	7.60E-04	4.95	181	6.85	48.47
D59047-11955	0.879	0.042	7.40E+04	<1E-05	<1	0.9962	4.13E+04	7.03E-04	18.00	176	5.8	-7.98
D70678-12637-S1	1.059	0.043	7.94E+03	<1E-05	<1	0.9289	3.48E+04	3.83E-04	11.13	196	3.875	67.80
D70678-12799-S1	1.489	0.043	6.83E+04	2.81E-04	4.12	0.8743	1.56E+04	2.43E-03	331.75	166	4.575	89.15
D70678-13531-S1	1.627	0.043	3.52E+04	<1E-05	<1	0.9954	5.93E+04	1.32E-04	2.38	149	3.375	55.47
D70678-13576-S1	1.134	0.043	3.04E+04	2.85E-04	9.38	0.9705	5.73E+04	1.60E-04	2.88	80	3.075	71.73
D70678-14004-S2	1.408	0.043	1.21E+04	<1E-05	<1	0.9456	1.98E+04	9.13E-04	47.75	95	2.9	40.60
D70678-14027-S2	1.510	0.043	2.63E+04	2.85E-04	10.8	0.9984	5.15E+04	3.85E-04	7.60	238	5.35	34.02
D70678-2155-S1	1.65	0.051	1.15E+04	<1E-05	<1	0.9966	4.55E+04	2.05E-04	4.63	225	4.975	35.94
D70678-2743-S1	1.496	0.044	5.33E+04	<1E-05	<1	0.9785	1.57E+04	2.00E-04	15.35	47	2.25	38.16
D70678-5521-S2	1.658	0.044	2.90E+04	<1E-05	<1	0.991	5.45E+04	1.60E-04	2.98	193	4.35	44.93

* Values <1E-05 (s-1) are beyond the limit of detection in this experiment and are estimated
** Values <1nM are beyond the limit of detection in this experiment and are estimated
*** Calculated as % increase or decrease in signal upon exposure of Antibody:S1 complex to 100nM ACE2 (as compared to Antibody:S1 signal)

sequence analysis was performed using the Geneious Biologics software. Screening results from a subset of representative candidates are shown in Table 1.

Concurrently, a single B cell discovery approach was employed whereby plasma cells were enriched from primary tissues prior to loading onto OptoSelect™ chips with the Berkeley Lights Beacon. Following single cell deposition into NanoPens, assay mixtures containing capture beads and fluorescently labeled target proteins were imported into the channels above the NanoPens. Throughout the course of the assay, antibody secreted from the plasma B cells diffused from the NanoPen chambers into the channel above. Upon bead binding, fluorescence from either directly labeled protein(s) or secondary detection antibodies was concentrated on the surface of the bead, resulting in the time-dependent development of fluorescent halos in the channels above the pens containing antigen-specific plasma cells (Figure 2). Plasma cells exhibiting on-Beacon binding profiles of interest were exported for immunoglobulin sequence capture and analysis with the Geneious Biologics software. The resulting naturally paired heavy and light chains were cloned into expression plasmids and recombinantly expressed. Purified antibodies were screened similarly to the strategy used for hybridoma candidates via ELISA and BLI with a subset of representative candidates displayed in Table 1.

High-throughput and high-content screening on lead candidates was performed on the Carterra LSA to elucidate kinetic profiles to the monovalent S1 protein (Table 1 and Figure 3). Full kinetic profiles were

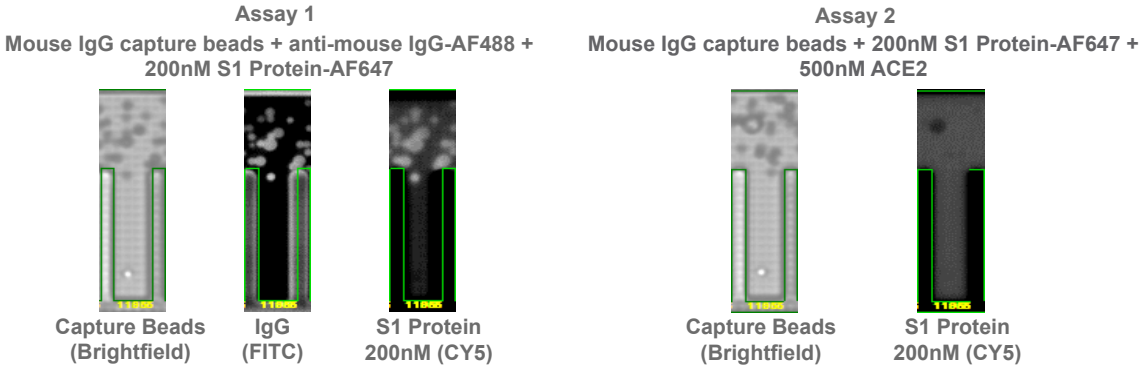

Figure 2. Example Beacon screening data for candidate D59047-11955. Anti-mouse IgG capture beads (brightfield image) were imported into the channel above the pens. Antibody secretion from a single B cell contained within a pen bound to capture beads at the mouth of the pen. In assay 1, antibody secretion was assessed by detection of total IgG in the FITC detection channel via binding of an anti-mouse IgG-AF488 conjugated secondary and simultaneously the specificity for S1 protein was determined in the CY5 detection channel with AF647 conjugated S1 protein at 200nM. In assay 2, binding competition between secreted antibody from the B cell and ACE2 receptor was assessed by precomplexing AF647-conjugated S1 protein with a molar excess of recombinant ACE2. A lack of antibody binding to S1 protein under these conditions demonstrated binding to a similar epitope as ACE2, thus indicative of a potential blocking candidate.

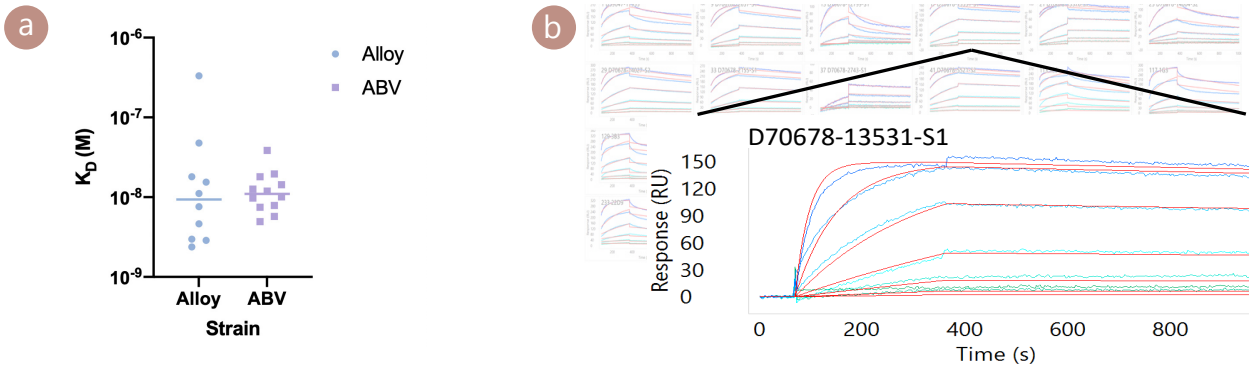

Figure 3. Carterra affinity analysis and example sensogram. With antibody captured on the chip surface, various concentrations of the target S1 protein were assessed for association and dissociation rates to calculate (a) final K_D values. (b) Array view of sensograms for each clone in the background with an example sensogram highlighted in the foreground. Each colored line indicates a distinct analyte concentration with red lines representing the curve fit analysis for rate constant calculations.

assessed in triplicate under regenerative and non-regenerative conditions with both purified antibodies and crude supernatant samples. Target S1 protein was used as an analyte in an ascending concentration series ranging from 0.49nM to 500nM with four-fold dilutions (Figure 3). All conditions (regeneration vs. non-regeneration and purified vs. crude antibody samples) yielded similar affinity values. The average resulting values from all asays is reported in Table 1.

Additionally, candidates were assayed on the Carterra LSA for the ability to block the S1:ACE2 binding interaction (Table 1 and Figure 4). ACE2 receptor blocking activity was interrogated by forming an antibody:S1 protein complex on the chip surface in a sequential format. Following complex formation, ACE2 was introduced as an analyte at 100nM (Figure 4) and the percent increase in RU value as a result of ACE2 binding was quantified using the RU signal from antibody:S1 complex formation as the baseline.

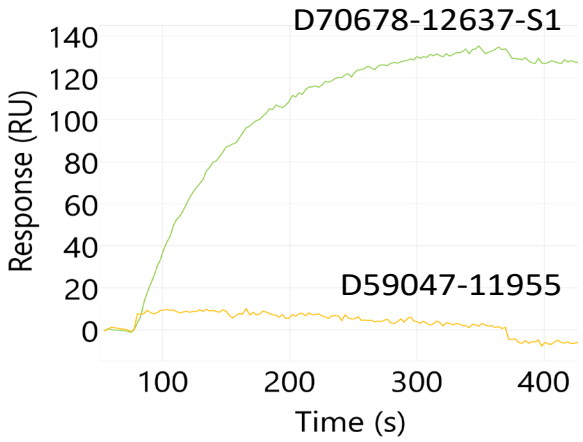

Figure 4. Example Carterra sensogram for antibody blocking of the S1:ACE2 interaction. Antibody:S1 protein complex was captured on the chip surface and ACE2 protein binding was assessed. A nonblocking candidate, D70678-12637-S1, complexed with S1 protein does not inhibit interaction with ACE2 (green). Conversely, a blocking candidate, D59047-11955, prevents ACE2 binding when S1 is complexed with the antibody (yellow).

a

S Protein		Avid Affinity (nM)	<1	<1	<1	<1	<1	<1	<1	<1	<1	10.8	<1	<1	4.12	14.2
S1 Protein		Monovalent Affinity (nM)	18.0	12.6	19.5	7.48	11.8	5.73	4.95	11.1	2.98	7.60	2.38	47.8	332	10.1
Avid Affinity (nM)	Monovalent Affinity (nM)	ID	1G3	16F2	21C3	18F4	22D9	1E5	3F2	D70678-12637-S1	D70678-5521-S2	D70678-14027-S2	D70678-13531-S1	D70678-14004-S2	D70678-12799-S1	3B3
1.25	9.73	23D11	0.70	0.68	0.48	0.44	0.98	0.89	1.30	1.29	1.56	1.63	1.54	1.33	1.34	1.53
<1	12.6	16F2	0.74		0.96	0.97	0.75	0.74	1.91	1.27	1.46	1.54	1.43	1.32	1.30	1.81
<1	7.48	18F4	0.39	0.48	0.09		0.41	0.53	0.58	1.55	1.45	1.43	1.62	1.27	1.48	0.77
<1	11.8	22D9	0.15	0.51	0.38	0.45		0.25	0.37	0.84	0.95	0.84	0.86	0.84	0.76	0.89
<1	5.73	1E5	0.39	0.52	0.68	0.63	0.49		0.65	1.17	1.25	1.27	1.15	1.10	1.12	1.39
<1	4.95	3F2	1.12	0.81	0.56	0.59	0.48	0.93		1.49	1.45	1.56	1.51	1.52	1.62	1.36
20.2	14.3	26E2	0.73	1.59	0.91	1.08	0.46	0.34	0.31	0.88	0.71	0.72	0.80	0.72	0.91	1.14
1.46	7.88	29F7	0.84	1.71	1.10	1.16	0.75	0.46	0.55	1.16	0.91	1.05	1.20	1.23	1.61	1.02
<1	2.98	D70678-5521-S2	1.75	0.84	2.65	1.31	3.38	1.88	7.21	1.31		1.41	1.04	1.42	1.31	4.55
10.8	7.60	D70678-14027-S2	0.96	1.03	0.91	0.87	1.04	1.36	1.19	1.57	0.75		0.97	1.04	1.60	1.27
<1	2.38	D70678-13531-S1	3.68	1.39	1.78	1.38	2.09	5.36	291.25	1.98	2.16	2.84		2.86	2.82	5.21
14.2	10.1	3B3	0.53	0.87	0.66	0.73	0.58	0.96	0.86	0.76	1.00	0.88	0.99	0.63	0.73	

ACE2 Blocking
ACE2 Intermediate Blocking
ACE2 Non-Blocking

Self-Self Interaction
Competitive Binding
Non-Competitive Binding

b

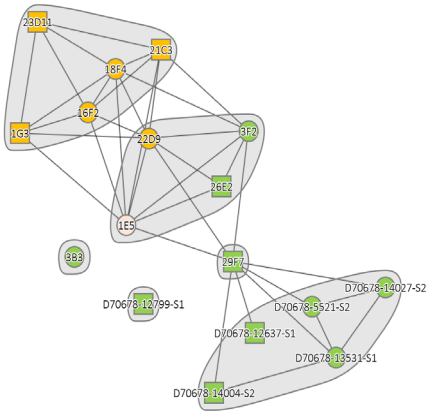

Figure 5. Select antibodies were characterized for competitive binding to the S1 protein to elucidate epitopic coverage. (a) All antibodies capable of binding S1 protein and preventing the S1:ACE2 interaction (ID highlighted in yellow) focused on a similar epitope (competitive binding indicated by red squares in grid). Antibodies that did not function as ACE2 blocking candidates (ID highlighted in light green) were distributed across two distinct core epitopes, with some antibodies binding at the interface of these epitopes, and an additional two clones appeared to bind distinct epitopes. Interestingly, an intermediate S1:ACE2 blocking candidate (1E5; ID highlighted in beige) bound at the interface between the ACE2 blocking epitope and a separate non-blocking epitope, thus supporting the partial blocking characteristic. No direct correlation was observed between affinity and binding epitope when assessed in either the monovalent binding format to the monomeric S1 protein or avid binding to the trimeric S protein. (b) A community network plot illustrates the bin clustering and distinct binding regions for each group of candidates.

The average of triplicate measurements is reported in Table 1. Non-blocking candidates resulted in a 50.8% ± 15.3% increase in signal from ACE2 binding, while blocking candidates completely prevented ACE2 binding (-1.96% ± 4.40% change in signal). One candidate, 1E5, demonstrated intermediate blocking characteristics with a 16.6% increase in signal upon ACE2 binding, perhaps indicative of a weak or partial blocking profile.

Lastly, candidate antibodies were assayed in a classical binning competition format (Figure 5) to identify the relative binding epitopes on the S1 protein. Epitope binning was performed on the Carterra LSA in a sequential format and binding of each antibody combination was assessed simultaneously. Non-competitive binding pairs and competitive binding pairs are highlighted by green or red squares, respectively, in Figure 5a (self interactions shown in dark red squares). The data is also presented as a community network plot in Figure 5b to better visualize the relative binding epitopes among the candidates assessed.

Sequence information for each candidate is presented in Table 2, including full paired heavy and light chain variable regions along with V-region and mutation rate analysis. Table 3 highlights common *in silico* liability assessment for each candidate based on published motifs[10,11] for antibodies.

Table 2. Heavy and light chain family and full sequence information for select characterized candidate antibodies.

ID	Mouse strain	Heavy V Gene	Heavy V Gene Identity %	VDJ Region
15G11	DivergimAb	IGHV1S137	98.64	QVQLQQSGAELVRPGVSVKISCKGSGYTFTDYAMHWVKQSHAKSLEWIGVISTYYGDASYNQKFKGKATMTVDKSSSTAYMELARLTSEDSAIYYCARWANWGYYYAMDYWGQGTSVTVSS
18F4	DivergimAb	IGHV2-9-1	100	QVQLKESGPGLVAPSQSLSITCTVSGFSLTSYAISWVRQPPGKGLEWLGVIWTGGGTNYNSALKSRLSISKDNSKSQVFLKMNSLQTDDTARYYCARKDYYGSSRNAMDYWGQGTSVTVSS
1E5	DiversimAb	IGHV1-55	100	QVQLQQPGAELVKPGASVKMSCKASGYTFTSYWITWVKQRPGQGLEWIGDIYPGSGSTNYNEKFKSKATLTVDTSSSTAYMQLSSLTSEDSAVYYCARSTVVATDAMDYWGQGTSVTVSS
1G3	DiversimAb	IGHV2-9-1	100	QVQLKESGPGLVAPSQSLSITCTVSGFSLTSYAISWVRQPPGKGLEWLGVIWTGGGTNYNSALKSRLSISKDNSKSQVFLKMNSLQTDDTARYYCARFHYYGSSYGYFDYWGQGTTLTVSS
21C3	DivergimAb	IGHV2-9-1	100	QVQLKESGPGLVAPSQSLSITCTVSGFSLTSYAISWVRQPPGKGLEWLGVIWTGGGTNYNSALKSRLSISKDNSKSQVFLKMNSLQTDDTARYYCARIYYGSSYFDYWGQGTTLTVSS
22D9	DivergimAb	IGHV1-54	100	QVQLQQSGAELVRPGTSVKVSCKASGYAFTNYLIEWVKQRPGQGLEWIGVINPGSGGTNYNEKFKGKATLTADKSSSTAYMQLSSLTSEDSAVYFCARRHYYYGVDYWGQGTTLTVSS
23D11	DivergimAb	IGHV1S113	97.22	EVQLQQSGPELVKPGASVKISCKTSGYTFTEYTMYWVKQSHGKSLEWIGGVNPNNGDTSYSQKFKGKATLTVDKSSSTAYMELRSLTSEDSAVYYCARDGYDLYYGMDYWGQGTSVTVSS
26E2	DivergimAb	IGHV14-4	100	EVQLQQSGAELVRPGASVKLSCTASGFNIKDDYMHWVKQRPEQGLEWIGWIDPENGDTEYASKFQGKATITADTSSNTAYLQLSSLTSEDTAVYYCTKGYYGSSYDYFDYWGQGTTLTVSS
29F7	DivergimAb	IGHV1-82	100	QVQLQQSGPELVKPGASVKISCKASGYAFSSSWMNWVKQRPGKGLEWIGRIYPGDGDTNYNGKFKGKATLTADKSSSTAYMQLSSLTSEDSAVYFCARDDYDEGDYWGQGTTLTVSS
3B3	DiversimAb	IGHV5-9-1	100	DVKLVESGEGLVKPGGSLKLSCAASGFTFSSYAMSWVRQTPEKRLEWVAYISSGGDYIYYADTVKGRFTISRDNARNTLYLQMSSLKSEDTAMYYCTRVARLYDGYFDYWGQGTTLTVSS
3F2	DiversimAb	IGHV14-4	97.95	EVQLQQSGAELVRPGASVKLSCTASGFNIKDDYMHWVKQRPEQGLEWIGWIDPENGDTEYASKFQGKATITVDISSNTAYLQLNSLTSEDTAVYYCSTLIYYYGSSNDYWGQGTTLTVSS
D59047-11955	DivergimAb	IGHV2-9-1	100	QVQLKESGPGLVAPSQSLSITCTVSGFSLTSYAISWVRQPPGKGLEWLGVIWTGGGTNYNSALKSRLSISKDNSKSQVFLKMNSLQTDDTARYYCARIYYYGSSYFDYWGQGTTLTVSS
D70678-12637-S1	Alloy	IGHV3-21	96.94	EVQLVESGGGLVKPGGSLRLSCATSGFTFSHYSMNWVRQAPGKGLEWVSSISSSSSNIYYADSVKGRFTVSRDNAKNSLYLQMNSLRAEDTAVYYCARRGSSWSFDYWGQGTLVTVSS
D70678-12799-S1	Alloy	IGHV1-2	97.95	QVQLVQSGAEVKKPGASVKVSCKASGYTFTDYYMHWVRQAPGQGLEWMGWINPNSGGTNYAQKFQGRVTMTRDTSISTAYMELSRLRSDDTALYYCARLDYWSQGTLVTVSS
D70678-13531-S1	Alloy	IGHV4-59	94.9	QVQLQESGPGLVKPSETLSLTCTVSGGSISSYYWTWIRQSPGKGLEWIGYIYYSGSTYTNPSLKSRVTFSVDTSENQFSLKLNSVTAADTAIYFCARDNMDVWGKGTTVTVSS
D70678-13576-S1	Alloy	IGHV4-59	94.58	QVQLQESGPGLVKPSETLSLTCTVSGGSISNYYWTWIRQPPGKGLEWIGYIYYSGSTYTNPSLKSRVTISVDTSENQFSLKLNSVTAADTAIYYCARDNMDVWGKGTTVTVSS
D70678-14004-S2	Alloy	IGHV1-18	97.64	QVQLVQSGAEVKKPGASVKVSCKASGYTFSSYGIIWVRQAPGQGLEWMGWISAYNGNTNYAQKLQGRVTMTTDTSTSTAYMELRTLRSDDTAVYYCAREITLNWNYAGWFDPWGQGTLVTVSS
D70678-14027-S2	Alloy	IGHV3-15	97.33	EVQLVESGGGLVKPGGSLRLSCAASGFTFSYAWMTWVRQAPGKGLEWVGRIKTKSDGGTTDYASPVKGKFTISRDDSKNTLYLQMNSLQTEDTAVYYCTTHSSPDYWGQGTLVTVSS
D70678-2155-S1	Alloy	IGHV3-15	94.06	QVQLVESGGDLVKPGGSLRLSCAASGFTFSNAWMTWVRQAPGKELEWVGRIKTKSDGGTIEYGVSVKGRFTISRDDSKNTLFLQMNSLTTEDTAVYYCTTHSSPDYWGQGTLVTVSS
D70678-2743-S1	Alloy	IGHV4-59	95.25	QVQLQESGPGLVKPSETLSLTCTVSGGSISSYYWTWIRQPPGKGLEWIGYIYSSGSTYTNPSLKSRVTISVDTSENQFSLKLNSVTAADTAVYYCARDNMDVWGKGTTVTVSS
D70678-5521-S2	Alloy	IGHV3-15	97	EVQLVESGGGLVKPGGSLRLSCAASGFTFNYAWMTWVRQAPGKGLDWVGRIKTKTDSGTTDYAAPVKGRFTISRDDSKNTLYLQMNNLKTEDTAVYYCTTHSTPDYWGQGTLVTVSS

ID	Mouse strain	Light V Gene	Light V Gene Identity %	VJ Region
15G11	DivergimAb	IGLV1	99.66	QAVVTQESALTTSPGETVTLTCRSSTGAVTTSNYANWVQEKPDHLFTGLIGGTNNRAPGVPARFSGSLIGDKAALTITGAQTEDEAIYFCALWYSNHWVFGGGTKLTVL
18F4	DivergimAb	IGLV1	100	QAVVTQESALTTSPGETVTLTCRSSTGAVTTSNYANWVQEKPDHLFTGLIGGTNNRAPGVPARFSGSLIGDKAALTITGAQTEDEAIYFCALWYSNHWVFGGGTKLTVL
1E5	DiversimAb	IGKV2-109	100	DIVMTQAAFSNPVTLGTSASISCRSSKSLLHSNGITYLYWYLQKPGQSPQLLIYQMSNLASGVPDRFSSSGSGTDFTLRISRVEAEDVGVYYCAQNLELPWTFGGGTKLEIK
1G3	DiversimAb	IGLV1	99.32	QAVVTQESALTTSPGETVTLTCRSSTGAVTTSNYANWVQEKPDHLFTGLIGGTNNRAPGVPARFSGSLIGDKAALTITGAQTEDEAIYFCALWYSNHWVFGGGTKLTVL
21C3	DivergimAb	IGLV1	99.66	QAVVTQESALTTSPGETVTLTCRSSTGAVTTSNYANWVQEKPDHLFTGLIGGTNNRAPGVPARFSGSLIGDKAALTITGAQTEDEAIYFCALWYSNQFIFGSGTKVTVL
22D9	DivergimAb	IGKV14-111	100	DIKMTQSPSSMYASLGERVTITCKASQDINSYLSWFQQKPGKSPKTLIYRANRLVDGVPSRFSGSGSGQDYSLTISSLEYEDMGIYYCLQYDELYTFGGGTKLEIK
23D11	DivergimAb	IGKV6-15	99.3	DIVMTQSQKFMSTSVGDRVSVTCKASQNVGTNVAWYQQKPGQSPKALIYSASYRYSGVPDRFTGSGSGTDFTLTISNVQSVDLAEYFCHQYNSYPWTFGGGTKLEIR
26E2	DivergimAb	IGKV19-93	99.65	DIQMTQSPSSLSASLGGKVTITCKASQDINKYIAWYQHKPGKGPRLLIHYTSTLQPGIPSRFSGSGSGRDYSFSISNLEPEDIATYYCLQYDNLWTFGGGTKLEIK
29F7	DivergimAb	IGKV6-15	100	DIVMTQSQKFMSTSVGDRVSVTCKASQNVGTNVAWYQQKPGQSPKALIYSASYRYSGVPDRFTGSGSGTDFTLTISNVQSEDLAEYFCQQYNSYPLYTFGGGTKLEIK
3B3	DiversimAb	IGKV3-10	100	NIVLTQSPASLAVSLGQRATISCRASESVDSYGNSFMHWYQQKPGQPPKLLIYLASNLESGVPARFSGSGSRTDFTLTIDPVEADDAATYYCQQNNEDPYTFGGGTKLEIK
3F2	DiversimAb	IGLV1	100	QAVVTQESALTTSPGETVTLTCRSSTGAVTTSNYANWVQEKPDHLFTGLIGGTNNRAPGVPARFSGSLIGDKAALTITGAQTEDEAIYFCALWYSNHWVFGGGTKLTVL
D59047-11955	DivergimAb	IGLV1	99.66	QAVVTQESALTTSPGETVTLTCRSSTGAVTTSNYANWVQEKPDHLFTGLIGGTNNRAPGVPARFSGSLIGDKAALTITGAQTEDEAIYFCALWYSNQFIFGSGTKVTVL
D70678-12637-S1	Alloy	IGKV3-20	97.19	EIVLTQSPATLSLSPGERAILSCRASQSISSTYLAWNQQKPGQAPRLLIYGASSRATGIPDRFSGSGSGTDFTLTISRLEPEDFAVYYCQQYGSSWTFGQGTKVEIK
D70678-12799-S1	Alloy	IGKV2-24	94.67	DIVMTQTPLSLPVTLGQPASISCRSSQSLVHSDGNTYLSWLQQRPGQPPRLLIYKISNRFSGVPDRFSGSGAGTDFTLKISRVEAEDVGVYYCMQETQFTWTFGQGTKVEIK
D70678-13531-S1	Alloy	IGKV2-30	97.99	DVVMTQTPLSLPVTLGQPASISCRCSQSLVYSDGNTYLNWFQQRPGQSPRRLIYKVSIRDSGVPDRFSGSGSGTDFTLKISRVEAEDVGIYYCMQGTHRPITFGRGTRLEIK
D70678-13576-S1	Alloy	IGKV4-1	94.7	DIVMTQSPDSLAVSLGERATINCKSSQSVLYSSNNKNYLAWYQQKPGQPPKLLIYWASTRESGVPDRFSGSGSGTDFTLTISSLQAEDVAVYYCQQYYSTPYTFGQGTKLEIK
D70678-14004-S2	Alloy	IGKV3-15	96.52	EIVMTQSPATLSVSPGERATLSCRASQSIRNNLAWYQQKPGQAPRLLIYGAISRATGVPARFSGSGSGTEFTLTISSLQSEDFAVYHCQQYNNWLPYTFGQGTKLEIK
D70678-14027-S2	Alloy	IGKV1-33;IGKV1D-33	99.3	DIQMTQSPSSLSASVGDRVTITCQASQDIRNYLNWYHQKPGKAPKLLIYDASNLETGVPSRFSGSGSGTDFTFTISSLQPEDIATYYCQQYDNLPYTFGQGTKLEIK
D70678-2155-S1	Alloy	IGKV1-33;IGKV1D-33	96.86	DIQMTQSPSSLSASVGDRVTITCQASQDIRNYLNWYQQKPGKAPKLLIYDASTLETGVPSRFSGSGSGTDFTFTISSLQPEDIATYYCHQYGNLPLSFGGGTKVEIK
D70678-2743-S1	Alloy	IGKV2-30	95.65	DVVMTQTPLSLPVTLGQPASISCRSSQSLVYSDGNTYLNWFQQRPGQSPRRLIYKVSNRDSGVPDRFSGSGSGTDFTLKISRVEAEDVGIYYCMQGTHWPIIFGRGTRLEIK
D70678-5521-S2	Alloy	IGKV1-33;IGKV1D-33	98.24	DIQMTQSPSSLSASVGDRVTITCQASQDINNHLNWYQQKPGKAPNLLIYDASNLETGVPSRFSGSGSGTDFTFTISSLQPEDFATYYCQQYDNLPYTFGQGTKLEIK

Table 3. *In silico* sequence analysis of candidate antibodies for common liability motifs.

ID	Mouse strain	Liability (High)	Liability (Medium)	Liability (Low)
15G11	DivergimAb	DS (Isomerization, Heavy FR3); M (Oxidation, Heavy CDR3)	TS (Cleavage, Heavy FR3, Heavy FR4); TS (Cleavage, Light CDR1, Light FR1); NH (Deamidation, Light CDR3)	SN (Deamidation, Light CDR1, Light CDR3); TN (Deamidation, Light CDR2)
18F4	DivergimAb	DP (Cleavage, IGHG2B); NA (Deamidation, Heavy CDR3); NS (Deamidation, 3 * Heavy FR3); M (Oxidation, Heavy CDR3)	TS (Cleavage, Heavy CDR1, Heavy FR4); TS (Cleavage, Light CDR1, Light FR1); NH (Deamidation, Light CDR3)	TN (Deamidation, IGHV2-9-1); SN (Deamidation, Light CDR1, Light CDR3); TN (Deamidation, Light CDR2)
1E5	DiversimAb	DS (Isomerization, Heavy FR3); M (Oxidation, Heavy CDR3); NG (Deamidation, Light CDR1); M (Oxidation, Light CDR2)	TS (Cleavage, Heavy CDR1, 2 * Heavy FR3, Heavy FR4); TS (Cleavage, Light FR1); NP (Hydrolysis, Light FR1)	TN (Deamidation, IGHV1-55); SN (Deamidation, IGKV2-109, Light CDR1, Light FR1)
1G3	DiversimAb	NS (Deamidation, 3 * Heavy FR3, IGHG1)	TS (Cleavage, Heavy CDR1); TS (Cleavage, Light CDR1, Light FR1); NH (Deamidation, Light CDR3)	TN (Deamidation, IGHG1, IGHV2-9-1); SN (Deamidation, Light CDR1, Light CDR3); TN (Deamidation, Light CDR2)
21C3	DivergimAb	NS (Deamidation, 3 * Heavy FR3)	TS (Cleavage, Heavy CDR1); TS (Cleavage, Light CDR1, Light FR1)	TN (Deamidation, IGHV2-9-1); SN (Deamidation, Light CDR1, Light CDR3); TN (Deamidation, Light CDR2)
22D9	DivergimAb	DS (Isomerization, Heavy FR3); NS (Deamidation, Light CDR1); DG (Isomerization, Light FR3)	TS (Cleavage, Heavy FR1, Heavy FR3); NH (Deamidation, IGHG1); NP (Hydrolysis, Heavy CDR2)	TN (Deamidation, Heavy CDR1, IGHV1-54)
23D11	DivergimAb	NG (Deamidation, Heavy CDR2); DG (Isomerization, Heavy CDR3); DS (Isomerization, Heavy FR3); M (Oxidation, Heavy CDR3); NS (Deamidation, Light CDR3)	TS (Cleavage, Heavy FR1, Heavy FR3, Heavy FR4, IGHV1S113); NP (Hydrolysis, Heavy CDR2); TS (Cleavage, Light FR1)	SN (Deamidation, Light FR3); TN (Deamidation, Light CDR1)
26E2	DivergimAb	DP (Cleavage, Heavy CDR2); NG (Deamidation, Heavy CDR2); DS (Isomerization, IGHG2A;IGHG2C)	TS (Cleavage, 2 * Heavy FR3, IGHG2A;IGHG2C)	SN (Deamidation, Heavy FR3); SN (Deamidation, Light FR3)
29F7	DivergimAb	NG (Deamidation, Heavy FR3); DG (Isomerization, Heavy CDR2); DS (Isomerization, Heavy FR3, IGHG2C); NS (Deamidation, Light CDR3)	TS (Cleavage, Heavy FR3); TS (Cleavage, Light FR1)	TN (Deamidation, IGHV1-82); SN (Deamidation, Light FR3); TN (Deamidation, Light CDR1)
3B3	DiversimAb	NA (Deamidation, Heavy FR3); DG (Isomerization, Heavy CDR3); DP (Cleavage, Light CDR3, Light FR3); NS (Deamidation, Light CDR1); DS (Isomerization, Light CDR1)		SN (Deamidation, IGKV3-10)
3F2	DiversimAb	DP (Cleavage, Heavy CDR2); NG (Deamidation, Heavy CDR2); NS (Deamidation, Heavy FR3);	TS (Cleavage, Heavy FR3); TS (Cleavage, Light CDR1, Light FR1); NH (Deamidation, Light CDR3)	SN (Deamidation, Heavy CDR3, Heavy FR3); SN (Deamidation, Light CDR1, Light CDR3); TN (Deamidation, Light CDR2)
D59047-11955	DivergimAb	NS (Deamidation, 3 * Heavy FR3)	TS (Cleavage, Heavy CDR1); TS (Cleavage, Light CDR1, Light FR1)	TN (Deamidation, IGHV2-9-1); SN (Deamidation, Light CDR1, Light CDR3); TN (Deamidation, Light CDR2)
D70678-12637-S1	Alloy	NA (Deamidation, Heavy FR3); NS (Deamidation, 2 * Heavy FR3); DS (Isomerization, Heavy FR3)	TS (Cleavage, Heavy FR1)	KN (Deamidation, Heavy FR3); SN (Deamidation, Heavy CDR2)
D70678-12799-S1	Alloy	NS (Deamidation, Heavy CDR2); DG (Isomerization, Light CDR1); M (Oxidation, Light CDR3)	TS (Cleavage, Heavy FR3); NP (Hydrolysis, Heavy CDR2)	TN (Deamidation, IGHV1-2); SN (Deamidation, IGKV2-24)
D70678-13531-S1	Alloy	NS (Deamidation, Heavy FR3); M (Oxidation, Heavy CDR3); 2 C (Extra Cysteine, Light FR1); DG (Isomerization, Light CDR1); DS (Isomerization, Light FR3); M (Oxidation, Light CDR3)	TS (Cleavage, Heavy FR3); NP (Hydrolysis, Heavy FR3)	TN (Deamidation, Heavy FR3)
D70678-13576-S1	Alloy	NS (Deamidation, Heavy FR3); M (Oxidation, Heavy CDR3); 2 C (Extra Cysteine, Light FR1); DG (Isomerization, Light CDR1); DS (Isomerization, Light FR3); M (Oxidation, Light CDR3); DS (Isomerization, Light FR1)	TS (Cleavage, Heavy FR3); NP (Hydrolysis, Heavy FR3)	SN (Deamidation, Heavy CDR1); TN (Deamidation, Heavy FR3); KN (Deamidation, Light CDR1); SN (Deamidation, Light CDR1)
D70678-14004-S2	Alloy	DP (Cleavage, Heavy CDR3); NG (Deamidation, Heavy CDR2);	TS (Cleavage, 2 * Heavy FR3)	TN (Deamidation, IGHV1-18)
D70678-14027-S2	Alloy	NS (Deamidation, Heavy FR3); DG (Isomerization, Heavy CDR2); DS (Isomerization, Heavy FR3);		KN (Deamidation, Heavy FR3); SN (Deamidation, IGKV1-33;IGKV1D-33)
D70678-2155-S1	Alloy	NA (Deamidation, Heavy CDR1); NS (Deamidation, Heavy FR3); DG (Isomerization, Heavy CDR2); DS (Isomerization, Heavy FR3);		KN (Deamidation, Heavy FR3); SN (Deamidation, Heavy CDR1)
D70678-2743-S1	Alloy	NS (Deamidation, Heavy FR3); M (Oxidation, Heavy CDR3); DG (Isomerization, Light CDR1); DS (Isomerization, Light FR3); M (Oxidation, Light CDR3)	TS (Cleavage, Heavy FR3); NP (Hydrolysis, Heavy FR3)	TN (Deamidation, Heavy FR3); SN (Deamidation, IGKV2-30)
D70678-5521-S2	Alloy	DS (Isomerization, Heavy CDR2, Heavy FR3)	NH (Deamidation, Light CDR1)	KN (Deamidation, Heavy FR3); SN (Deamidation, IGKV1-33;IGKV1D-33)

Discussion

The COVID-19 pandemic highlighted the importance of rapid discovery of antiviral drugs, both prophylactic and therapeutic, as critical to containing the spread of the virus.[12] In response to the COVID-19 outbreak, the scientific community collectively answered the public health call to action with extraordinary momentum, leveraging both new and traditional technologies with a strong emphasis on speed.[13] Continuing to build on COVID-19 research critical to public health while highlighting various methods that can be deployed for antibody discovery, this report outlines the use of a number of distinct workflows that enabled the accelerated identification of antiviral antibodies, some with promising therapeutic potential. The sequence information and corresponding characterization data for a panel of 21 antibody candidates is reported for unrestricted use.

We highlight the use of both DiversimAb and Alloy GK mice in accelerated hybridoma-based and single B cell screening platforms. To enable rapid generation of monoclonal antibodies out of the DiversimAb platform, mice were immunized on a 16-day accelerated schedule followed by hybridoma generation.

Concurrently, Alloy mice were immunized on a 5-week schedule and subsequently screened on the Beacon in a single day followed by a sequence recovery and analysis process spanning less than one week. Despite the divergent immunization and screening workflows, both campaigns yielded sequences in similar timeframes to enable simultaneous downstream characterization requiring three total days. In sum, both campaigns required fewer than three months from immunization start to fully-characterized, purified antibody. Of course, alternative workflows are possible to further tighten the timeline for future campaigns. For example, characterization data was acquired using both purified and crude antibody samples to validate either source on the Carterra LSA for kinetic, neutralization and binning data. With equivalent results, the time and resources required for purification can be incorporated further downstream to expedite the early discovery timeline. In addition, Alloy mice can be immunized on a more accelerated timeline.

The resulting data set presented here is comprised of a diverse panel of candidate antibodies spanning multiple epitopes with high affinity and both receptor blocking and non-blocking activity. Interestingly, all candidate antibodies identified from the Alloy mice fell within a similar non-blocking bin, likely indicative of epitope immunodominance,[14] which has been reported as a common result from COVID-19 infection.[15,16] However, the extended immunization strategy employed for the Alloy mice resulted in high affinity antibodies, including the top four highest affinity candidates presented here. The balance between diversity and affinity is a challenge for *in vivo* immunization models: with continued boosting, clonal expansion of the highest affinity germline B cells can often result in a limited overall diversity.[17] Alternative immunization workflows involving rapid schedules and/or immunogen manipulation are effective risk mitigation strategies to circumvent these challenges.[18] In this case, the DiversimAb mice were immunized following an accelerated strategy to maximize epitopic diversity, and although the overall average affinity of these candidates was lower as a result, a subset of high affinity blocking clones were discovered. It is also important to note that recent studies have identified non-blocking neutralizing epitopes,[19] indicating further testing of non-blocking Alloy candidates identified here could reveal efficacious potential in viral neutralizing experiments.

A review of the lead candidate sequences further underscores the importance of risk mitigation in antibody discovery through the use of multiple strains of mice for added diversity. It is well documented that genetic backgrounds heavily influence the B cell repertoire diversity.[20,21] Therefore, in cases where rapid discovery is imperative, starting with multiple strains can improve the diversity in gene usage for V(D)J recombination. In the case of the Abveris DiversimAb mice, two separate background strains were leveraged (DiversimAb vs. DivergimAb) to further increase the output sequence diversity. Interestingly, many of the candidates from these mice contained near germline V-regions; likely a result of the accelerated immunization approach employed for rapid discovery. Regardless, binding affinity is still maintained at the nanomolar level, which could be due to the unique and diverse CDR3 regions. The presence of germline sequences from DiversimAb mice using this immunization approach provides an opportunity for streamlined lead optimization via humanization and affinity maturation without the need to assess numerous V region backmutation permutations.

Traditional methods of *in vivo* antibody drug discovery suffer from timeline disadvantages associated with immunization, humanization, and downstream lead optimization (if required).[22] However, with the recent development of innovative new technologies to accelerate the upstream drug discovery process highlighted in this report, *in vivo* antibody discovery is now a viable option for an accelerated response to novel viral threats. Humanized mouse strains can be leveraged synergistically with genetically engineered mice designed to increase epitopic diversity (DiversimAb) to provide lead and backup antibody drug candidates of desired therapeutic efficacy. When combined with efficient high-throughput downstream antibody capture and characterization tools, it becomes possible to go from immunization to sequence in as few as 29 days.

References

1. Huang C, Wang Y, Li X, Ren L, Zhao J, Hu Y, Zhang L, Fan G, Xu J, Gu X, Cheng Z, Yu T, Xia J, Wei Y, Wu W, Xie X, Yin W, Li H, Liu M, Xiao Y, Gao H, Guo L, Xie J, Wang G, Jiang R, Gao Z, Jin Q, Wang J, Cao B. Clinical features of patients infected with 2019 novel coronavirus in Wuhan, China. Lancet. 2020 Feb 15;395(10223):497-506. doi: 0.1016/S0140-6736(20)30183-5.

2. Fineberg HV. Pandemic preparedness and response--lessons from the H1N1 influenza of 2009. N Engl J Med. 2014 Apr 3;370(14):1335-42. doi: 10.1056/NEJMra1208802.

3. Furuyama W, Marzi A, Nanbo A, Haddock E, Maruyama J, Miyamoto H, Igarashi M, Yoshida R, Noyori O, Feldmann H, Takada A. Discovery of an antibody for pan-ebolavirus therapy. Sci Rep. 2016 Feb 10;6:20514. doi: 10.1038/srep20514.

4. Bornholdt ZA, Turner HL, Murin CD, Li W, Sok D, Souders CA, Piper AE, Goff A, Shamblin JD, Wollen SE, Sprague TR, Fusco ML, Pommert KB, Cavacini LA, Smith HL, Klempner M, Reimann KA, Krauland E, Gerngross TU, Wittrup KD, Saphire EO, Burton DR, Glass PJ, Ward AB, Walker LM. Isolation of potent neutralizing antibodies from a survivor of the 2014 Ebola virus outbreak. Science. 2016 Mar 4;351(6277):1078-83. doi: 10.1126/science.aad5788.

5. Lowe R, Barcellos C, Brasil P, Cruz OG, Honório NA, Kuper H, Carvalho MS. The Zika Virus Epidemic in Brazil: From Discovery to Future Implications. Int J Environ Res Public Health. 2018 Jan 9;15(1):96. doi: 10.3390/ijerph15010096.

6. Klasse PJ. Neutralization of Virus Infectivity by Antibodies: Old Problems in New Perspectives. Adv Biol. 2014;2014:157895. doi: 10.1155/2014/157895.

7. Correia BE, Bates JT, Loomis RJ, Baneyx G, Carrico C, Jardine JG, Rupert P, Correnti C, Kalyuzhniy O, Vittal V, Connell MJ, Stevens E, Schroeter A, Chen M, Macpherson S, Serra AM, Adachi Y, Holmes MA, Li Y, Klevit RE, Graham BS, Wyatt RT, Baker D, Strong RK, Crowe JE Jr, Johnson PR, Schief WR. Proof of principle for epitope-focused vaccine design. Nature. 2014 Mar 13;507(7491):201-6. doi: 10.1038/nature12966.

8. Ali MG, Zhang Z, Gao Q, Pan M, Rowan EG, Zhang J. Recent advances in therapeutic applications of neutralizing antibodies for virus infections: an overview. Immunol Res. 2020 Dec;68(6):325-339. doi: 10.1007/s12026-020-09159-z.

9. VanBlargan LA, Goo L, Pierson TC. Deconstructing the Antiviral Neutralizing-Antibody Response: Implications for Vaccine Development and Immunity. Microbiol Mol Biol Rev. 2016 Oct 26;80(4):989 1010. doi: 10.1128/MMBR.00024-15.

10. Lu X, Nobrega RP, Lynaugh H, Jain T, Barlow K, Boland T, Sivasubramanian A, Vásquez M, Xu Y. Deamidation and isomerization liability analysis of 131 clinical-stage antibodies. MAbs. 2019 Jan;11(1):45-57. doi: 10.1080/19420862.2018.1548233.

11. Xu A, Kim HS, Estee S, ViaJar S, Galush WJ, Gill A, Hötzel I, Lazar GA, McDonald P, Andersen N, Spiess C. Susceptibility of Antibody CDR Residues to Chemical Modifications Can Be Revealed Prior to Antibody Humanization and Aid in the Lead Selection Process. Mol Pharm. 2018 Oct 1;15(10):4529-4537. doi: 10.1021/acs.molpharmaceut.8b00536.

12. Zhu Y, Li J, Pang Z. Recent insights for the emerging COVID-19: Drug discovery, therapeutic options and vaccine development. Asian J Pharm Sci. 2021 Jan;16(1):4-23. doi: 10.1016/j.ajps.2020.06.001.

13. Sempowski GD, Saunders KO, Acharya P, Wiehe KJ, Haynes BF. Pandemic Preparedness: Developing Vaccines and Therapeutic Antibodies For COVID-19. Cell. 2020 Jun 25;181(7):1458-1463. doi: 10.1016/j.cell.2020.05.041.

14. Angeletti D, Yewdell JW. Understanding and Manipulating Viral Immunity: Antibody Immunodominance Enters Center Stage. Trends Immunol. 2018 Jul;39(7):549-561. doi: 10.1016/j.it.2018.04.008.

15. Andreano E, Rappuoli R. Immunodominant antibody germlines in COVID-19. J Exp Med. 2021 May 3;218(5):e20210281. doi: 10.1084/jem.20210281.

16. Farrera-Soler L, Daguer JP, Barluenga S, Vadas O, Cohen P, Pagano S, Yerly S, Kaiser L, Vuilleumier N, Winssinger N. Identification of immunodominant linear epitopes from SARS-CoV-2 patient plasma. PLoS One. 2020 Sep 9;15(9):e0238089. doi: 10.1371/journal.pone.0238089.

17. Mesin L, Schiepers A, Ersching J, Barbulescu A, Cavazzoni CB, Angelini A, Okada T, Kurosaki T, Victora GD. Restricted Clonality and Limited Germinal Center Reentry Characterize Memory B Cell Reactivation by Boosting. Cell. 2020 Jan 9;180(1):92-106.e11. doi: 10.1016/j.cell.2019.11.032.

18. Asensio MA, Lim YW, Wayham N, Stadtmiller K, Edgar RC, Leong J, Leong R, Mizrahi RA, Adams MS, Simons JF, Spindler MJ, Johnson DS, Adler AS. Antibody repertoire analysis of mouse immunization protocols using microfluidics and molecular genomics. MAbs. 2019 Jul;11(5):870-883. doi: 10.1080/19420862.2019.1583995.

19. Yu F, Xiang R, Deng X, Wang L, Yu Z, Tian S, Liang R, Li Y, Ying T, Jiang S. Receptor-binding domain-specific human neutralizing monoclonal antibodies against SARS-CoV and SARS-CoV-2. Signal Transduct Target Ther. 2020 Sep 22;5(1):212. doi: 10.1038/s41392-020-00318-0.

20. Chaaya N, Shahsavarian MA, Maffucci I, Friboulet A, Offmann B, Léger JB, Rousseau S, Avalle B, Padiolleau-Lefèvre S. Genetic background and immunological status influence B cell repertoire diversity in mice. Sci Rep. 2019 Oct 3;9(1):14261. doi: 10.1038/s41598-019-50714-y.

21. Greiff V, Menzel U, Miho E, Weber C, Riedel R, Cook S, Valai A, Lopes T, Radbruch A, Winkler TH, Reddy ST. Systems Analysis Reveals High Genetic and Antigen-Driven Predetermination of Antibody Repertoires throughout B Cell Development. Cell Rep. 2017 May 16;19(7):1467-1478. doi: 10.1016/j.celrep.2017.04.054.

22. Lu RM, Hwang YC, Liu IJ, Lee CC, Tsai HZ, Li HJ, Wu HC. Development of therapeutic antibodies for the treatment of diseases. J Biomed Sci. 2020 Jan 2;27(1):1. doi: 10.1186/s12929-019-0592-z.